Check for updates

Inorganic molecule (O$_2$, NO) adsorption on nitrogen- and phosphorus-doped MoS$_2$ monolayer using first principle calculations†

Hafiz Ghulam Abbas, [ID] [a] Tekalign Terfa Debela, [ID] [b] Sajjad Hussain*[c] and Iftikhar Hussain[d]

We performed a systematic study of the adsorption behaviors of O$_2$ and NO gas molecules on pristine MoS$_2$, N-doped, and P-doped MoS$_2$ monolayers *via* first principle calculations. Our adsorption energy calculations and charge analysis showed that the interactions between the NO and O$_2$ molecules and P–MoS$_2$ system are stronger than that of pristine and N–MoS$_2$. The spin of the absorbed molecule couples differently depending on the type of gas molecule adsorbed on the P- and N-substituted MoS$_2$ monolayer. Meanwhile, the adsorption of O$_2$ molecules leaves N- and P–MoS$_2$ a magnetic semiconductor, whereas the adsorption of an NO molecule turns this system into a nonmagnetic semiconductor, which may provide some helpful information for designing new N- and P-substituted MoS$_2$-based nanoelectronic devices. Therefore, P- and N–MoS$_2$ can be used to distinguish O$_2$ and NO gases using magnetic properties, and P–MoS$_2$-based gas sensors are predicted to be more sensitive to detect NO molecules rather than pristine and N–MoS$_2$ systems.

1. Introduction

Graphene, a single atomic layer of carbon atoms arranged in a hexagonal network, has drawn significant attraction from the scientific community due to its remarkable properties, and therefore has been efficiently implemented in electronics, energy devices, and gas sensors.[1–4] However, it is known that graphene is a semi-metal with no bandgap by nature, chemically inert, and has intrinsic defects, making it less fascinating for some applications. Particularly, graphene-based gas sensors have achieved a sensitivity down to the single molecule level. In the last few years, the semiconducting relationship between graphene and molybdenum disulfide (MoS$_2$) has drawn great attention, which results in excellent nanoelectronic, optoelectronics and energy harvesting properties.[5] Nevertheless, the zero band gap of graphene also limits its application in low-power electronics and digital circuits. Recently, considerable interest has been focused on layered transition metal dichalcogenides (LTMDs), especially monolayer molybdenum

disulfide (MoS$_2$). MoS$_2$ offers an attractive semiconductor option due to its direct band gap (~1.74 eV), ideal subthreshold swing of ~60 mV dec^{-1}, high current on/off ratio (10^8) and large in-plane carrier mobility of (~200 cm^2 V^{-1} S^{-1}) at room temperature, which shows potential for transistor applications.[6,7]

Owing to its high surface to volume ratio, monolayer MoS$_2$ can be considered the best candidate for gas sensing. It has already been demonstrated that gas sensors based on MoS$_2$ have higher sensitivity for NO$_2$ gas than graphene oxide field-effect transistor sensors. Consequently, below the 0.8 ppm detection limit, MoS$_2$-based gas sensors show more sensitivity for NO gas.[7,8] Previous research results have shown that the adsorption of gas molecules is physisorption on pristine MoS$_2$ and graphene monolayers.[9,10] Their gas sensitivity can be enhanced by introducing sulfur vacancies or dopants.[11,12] For instance, metal and non-metal dopants significantly improve the gas sensing performance of graphene.[13,14] On the other hand, Au, Fe, Co, and Ni-doped MoS$_2$ monolayers increase the gas sensitivity for CO, NO, and O$_2$ molecules.[15–17] Similar to the case of graphene, dopants can play a key role in tuning the electronic structure properties and chemical reactivity of monolayer MoS$_2$.[18–21] Moreover, various defects can be induced in MoS$_2$, as confirmed from previous experiments and theoretical calculations.[22–24] Molecular doping at sulfur vacancies can be introduced reliably by electron irradiation, which provides an efficient way to tailor the properties of MoS$_2$.[25,26] Therefore, it is very interesting to explore the electronic properties of defective MoS$_2$ monolayer *via* the adsorption of gas

^{a}Department of Nanoscience and Nanotechnology, Research Institute of Physics and Chemistry, Chonbuk National University, Chonbuk 561-756, Jeonju, Republic of Korea
^{b}Institute for Application of Advanced Material, Jeonju University, Chonju Chonbuk 55069, Republic of Korea
^{c}Department of Nano and Advanced Materials Engineering, Sejong University, Seoul 143-747, Republic of Korea. E-mail: shussainawan@gmail.com; hussain@sejong.ac.kr
^{d}School of Chemical Engineering, Yeungnam University, Gyeongsan, Gyeongbuk 38541, Republic of Korea

† Electronic supplementary information (ESI) available. See DOI: 10.1039/c8ra07638c

molecules. Accordingly, several theoretical works have reported the interaction between small inorganic (CO_2, NO, CO, H_2O, NO, NO_2, H_2, and N_2) gas molecules with pristine and defective MoS_2, and an enhancement in reactivity was also observed *via* NO_2 molecule adsorption at the edges of MoS_2.[27–29] To the best of our knowledge, the effect of different gas molecules (O_2 and NO) has not been demonstrated on doped monolayers MoS_2 due to the lack of detailed experimental studies.[13,30] Moreover, under experimental conditions, factors such as ambient water and oxygen may significantly affect the performance of field-effect transistors composed of MoS_2 monolayers.[31] Currently, it is obvious that toxic gases are a major challenge in the environmental pollution problem. Therefore, the study of gas molecule adsorption, identifying the best gas sensors such as MoS_2-based gas sensors, and their fabrication play a pivotal role in detecting toxic gas molecules.

We chose P-doped and N-doped atoms as dopants because inert sulfur (S) atoms cover the active sites of Mo atoms, causing poor chemical reactivity of the pristine MoS_2 in most stable 2H phase. The dopants enhance the conductivity of the system, tailor its electronic properties and improve the bonding of gas molecules on MoS_2. In addition, P–MoS_2 and N–MoS_2 doping has been observed experimentally,[32,33] and their formation energies indicate that they can be easily incorporated into an MoS_2 monolayer. Moreover, P and S atoms have a similar covalent radius and belong to the same family, which suggest that they may easily form stable chemical bonds with Mo atoms. NO gas is the main air pollutant generated from the combustion of nitrogen and oxygen in the atmosphere, and its existence causes serious health problems. Therefore, the measurement of the concentration of oxygen and NO in the environment is of special interest and importance. Herein, we investigate NO and O_2 gas molecule adsorption on pristine, N- and P-doped monolayer MoS_2 using first principle calculations. It was probed that N- and P-doped MoS_2 have high chemical stability. As a result, the electronic structure and charge analysis of N and P-doped MoS_2 suggest that these systems are promising candidates for the sensing of gas molecules and as alternative catalysts to the graphene system.

2. Computational details

Geometry optimizations were performed using the Vienna ab initio simulation package (VASP).[34,35] The electron–ion interactions were described using the projector-augmented wave (PAW) method, which is primarily a frozen-core all-electron calculation.[35] Attractive van der Waals interactions were included using the Grimme correction for the PBE-D3 method.[36] For structure optimization, atoms were relaxed in the direction of the Hellmann–Feynman force using the conjugate gradient method with an energy cut-off of 400 eV until a stringent convergence criterion (of 0.02 eV $Å^{-1}$) was satisfied. Lattice constants were optimized using the PBE-D3 exchange-correlation functional. The accurate electronic structure calculations were performed using the PBE-D3 exchange-correlation functional.[37] To simulate a low-dimensional MoS_2 sheet, we used a 4 × 4 supercell model consisting of 32 atoms in the *XY*

plane, where the optimized lattice constant along the two directions was 12.64 Å. The *k*-point sampling was done using Gamma centered 8 × 8 × 1 *k*-points.

3. Results and discussion

Before we studied the adsorption of gas molecules on pristine, N- and P-substituted MoS_2 monolayers, it was important to explore their electronic structure and structural stability based on their formation energies. The formation energy (E_{from}) can be calculated from the relation:

$$E_{form} = E_{tot}(MoS_2–X) - E_{tot}(MoS_2) + n(\mu_S) - m(\mu_X)$$

where, $E_{tot}(MoS_2–X)$, $E_{tot}[MoS_2]$, μ_S and μ_X are the total energy of monolayer MoS_2 substituted with N and P atoms, the total energy of the pristine MoS_2, and the chemical potential of individual S, N and P atoms in bulk FCC phases, n and m denote the number of S, N and P atoms, respectively. The formation energy of P- and N-substituted MoS_2 monolayer is −0.22 and −2.79 eV, respectively. The smaller the E_{from}, the better stability of the structure. Fig. 1(a) and (b) represent the chemical structure of the N- and P-substituted (4 × 4) supercells of the MoS_2 monolayer. In the optimized structure of N–MoS_2, the average bond length between the Mo–N atoms is 2.08 Å and the N atom sinks 0.78 Å below the MoS_2 plane along the *Z*-axis, which is consistent with theoretically reported values.[32–42] Therefore, this indicates the formation of a strong chemical bond between the N and Mo atoms. The average bond length for the Mo–P atoms is 2.41 Å (2.44 Å),[42–44] which is close to the bond length of the Mo–S atoms. The substitution of N and P atoms in the (4 × 4) supercell of the MoS_2 monolayer produced a magnetic moment $0.77\mu_B$ and $0.72\mu_B$, respectively. Fig. 1(c) and (d) exhibit the spin-density ($\rho\uparrow-\rho\downarrow$) iso-surface and it shows that the spin transferred from the substituted N and P atoms to the neighboring Mo atoms, where the spin accumulation and depletion regions are represented by red and green colors, respectively.

To explore the electronic properties of the pristine N and P substituted (4 × 4) MoS_2 monolayer, spin and non-spin-polarized band structure calculations were performed, and their band structures are shown in Fig. 2(a)–(c). The spin total density of states (TDOS) and spin partial density of states (PDOS) projected to the atomic orbital of the N and P atoms as well as the neighboring Mo atoms are shown in Fig. S2 and S3,† respectively. The pristine MoS_2 monolayer shows nonmagnetic semiconductor character and has a direct band gap of 1.74 eV, which is consistent with reported values.[38] Compared with the pristine MoS_2 monolayer, there are two localized electronic state locates around the Fermi-level in the band structure of N–MoS_2 and P–MoS_2, which are a result of the strong interaction between the N, P and Mo atoms. The pristine MoS_2 monolayer conduction band mainly consists of d-states of Mo, while its valence band contains a combination of d-Mo and p-S states. The existence of a localized defect state near the valence band maximum is due to the strong hybridization with neighboring dz^2 (Mo) and substituted pz (N) and pz (P) states, as shown in Fig. S2 and S3,† respectively. We observed that the substituted-
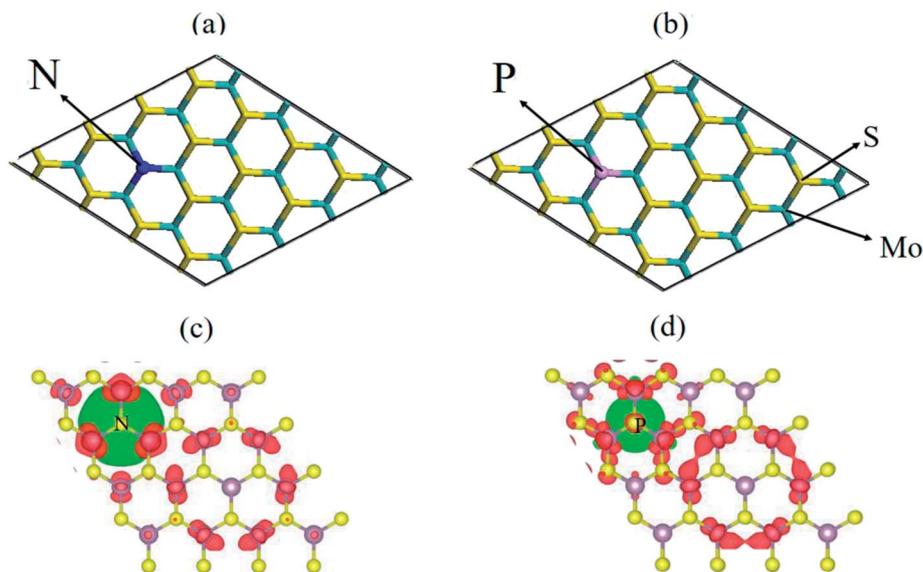
Fig. 1 Top-view (a and b) chemical structure of the N- and P-doped (4 × 4) MoS_2 monolayer, where the violet, yellow, green, and purple sticks represent the Mo, S, N and P atoms, respectively. (c and d) Spin-density ($\rho\uparrow - \rho\downarrow$) iso-surface plots for the N- and P-doped MoS_2 monolayer, where the spin accumulation and depletion regions are represented by red and green colors, respectively.

atom p states are spin-polarized, which play an important role in the system magnetism. The presence of N and P atoms causes degeneracy in the band structure of the N–MoS_2 and P–MoS_2 monolayers, which changes the symmetry of the system. Our Bader charge analysis showed that there is 0.30 and $0.91e^-$

charge transferring from monolayer MoS_2 to the N and P atoms, which is consistent earlier reported values.[12] Notably, we observed that p-type doping is achieved with N- and P-substituted atoms, which is consistent with experimental predictions.[32,33]
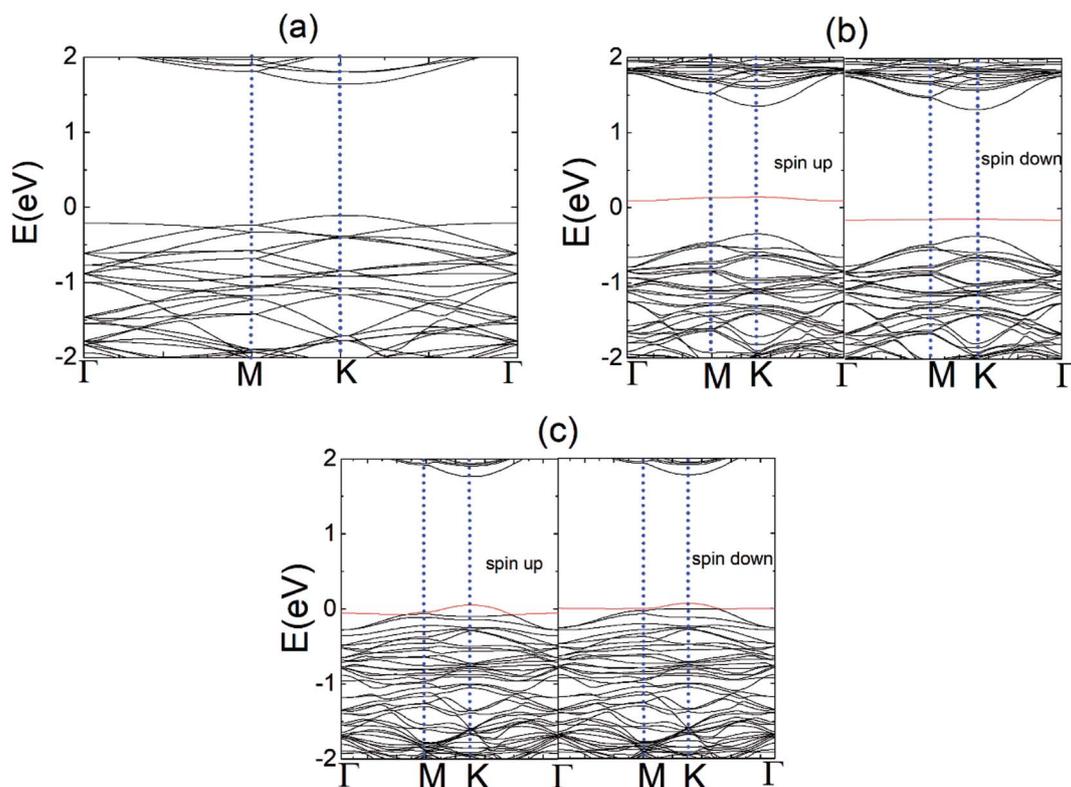
Fig. 2 Band structures of (a) monolayer pristine MoS_2, (b) N–MoS_2 for the spin-up and spin-down states, and (c) P–MoS_2 for the spin-up and spin-down states. The red line represents the state of the dopant atoms.

Table 1 Parameters of the (4 × 4) MoS_2 monolayer with adsorbed O_2 or NO molecules

Absorbent	Adsorbate (AB)	$E_{ad}{}^a$ (eV)	$L_{X-B}{}^d$ (Å)	$L_o{}^b$ (Å)	L^c (Å)	ΔQ^e (e)	μ (μ_B)
MoS_2	O_2	−0.01	3.38	1.24	1.24	0.03	1.62
$N-MoS_2$	O_2	−0.32	1.68	—	1.27	0.21	0.83
$2N-MoS_2$	$2O_2$	−0.22	1.50	—	1.30	0.40	1.68
$P-MoS_2$	O_2	−1.27	1.65	—	1.57	0.25	0.80
$2P-MoS_2$	$2O_2$	−1.22	1.65	—	1.57	0.40	1.62
MoS_2	NO	−0.26	3.03	1.17	1.17	—	0.69
$N-MoS_2$	NO	−0.56	2.20	—	1.15	0.11	NM
$2N-MoS_2$	2NO	−0.37	2.18	—	1.14	0.24	NM
$P-MoS_2$	NO	−1.44	1.93	—	1.20	0.14	NM
$2P-MoS_2$	2NO	−1.38	1.93	—	1.20	0.28	NM

[a] The adsorption energy per gas molecule to the pristine and N- or P-atom substituted MoS_2 surface. [b] Interatomic distance of the adsorbed gas molecule before adsorption. [c] Interatomic distance of the adsorbed gas molecule after adsorption. [d] The interatomic distance between doped (X = S, N or P) and atom B of the adsorbed molecule. B represents the O or N atom when the adsorbed molecule is O_2 or NO, respectively. [e] The total charge transfer from the MoS_2 monolayer to the gas molecules. The amount of total charge transfer was defined as: $\Delta Q = Q_{max} - Q_{min}$, where Q_{max} and Q_{min} correspond to the maximum and minimum charge values in the regions adjacent to the MoS_2 layers and $m(O_2$ and NO), respectively.

Next, we delved into the adsorption of triplet molecular oxygen ($^3O_2$) on the pristine MoS_2 monolayer. Accordingly, we calculated the adsorption of an oxygen molecule on the pristine MoS_2. We considered two different attachments of the O_2 gas molecule. In the parallel attachment (P), the two oxygen atoms of the O_2 gas molecule are parallel to the MoS_2 plane on the top of the sulfur atoms, while they are located on the MoS_2 plane in the vertical attachment (V) on the top of the sulfur atom. Our calculation showed that the former configuration in the MoS_2 monolayer is more stable than the latter by (0.04 eV). Therefore, our description will concentrate on P configurations.

Table 1 compares the adsorption energies (E_{ad}) of the gas molecule for various configurations from the PBE-D3 calculations. Here, E_{ad} is defined by the relation: $E_{ad} = E_T(MoS_2-O_2) -$ $E_T(MoS_2) - E_T(O_2)$, where E_T is the total energy of an appropriate system. Here, the total energy of the complex and isolated O_2 was obtained from the spin-polarized calculation. The configuration in which the O_2 molecule is adsorbed on the MoS_2 monolayer is indicated by its lower adsorption energy (−10 meV), which indicate weak physisorption between the O_2 molecule and pristine single-layer MoS_2. The O–O bond length is 1.24 Å, which remains the same as in the gas phase, which is also consistent with previous studies.[13] Our charge analysis showed that a very small charge (0.03e) transfer from the MoS_2 monolayer to the π^* states of the O_2 molecule. The adsorption energy of O_2 on the pristine MoS_2 monolayer is consistent with other reported values using the LDA and PBE-D3 functionals.[13–45] Here, it is important to compare the adsorption
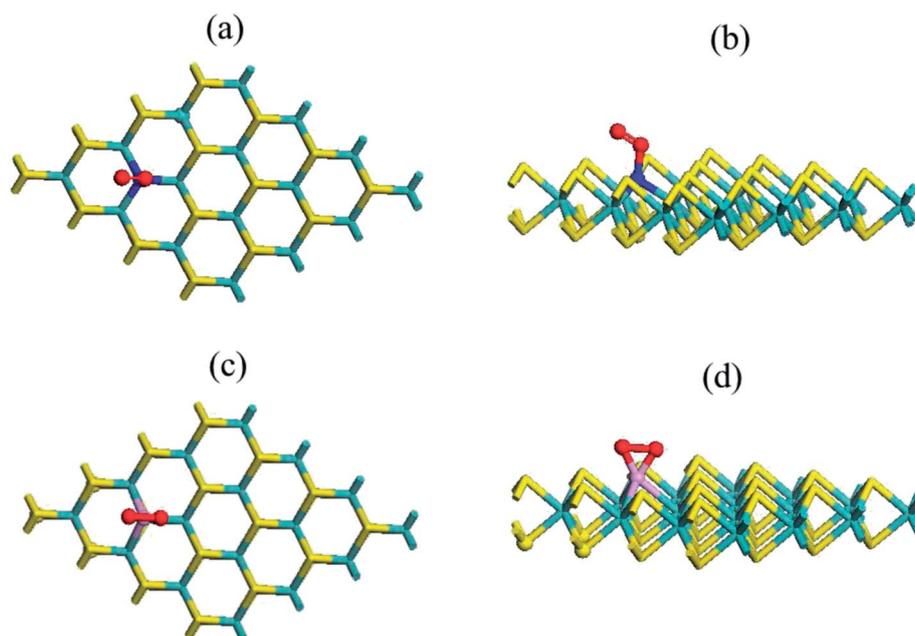

Fig. 3 Top (a and c) and side (b and d) views of the chemical structure of the N- and P-substituted MoS_2-O_2 complex, where violet, yellow, green, red and purple sticks represent the Mo, S, N, O and P atoms, respectively.
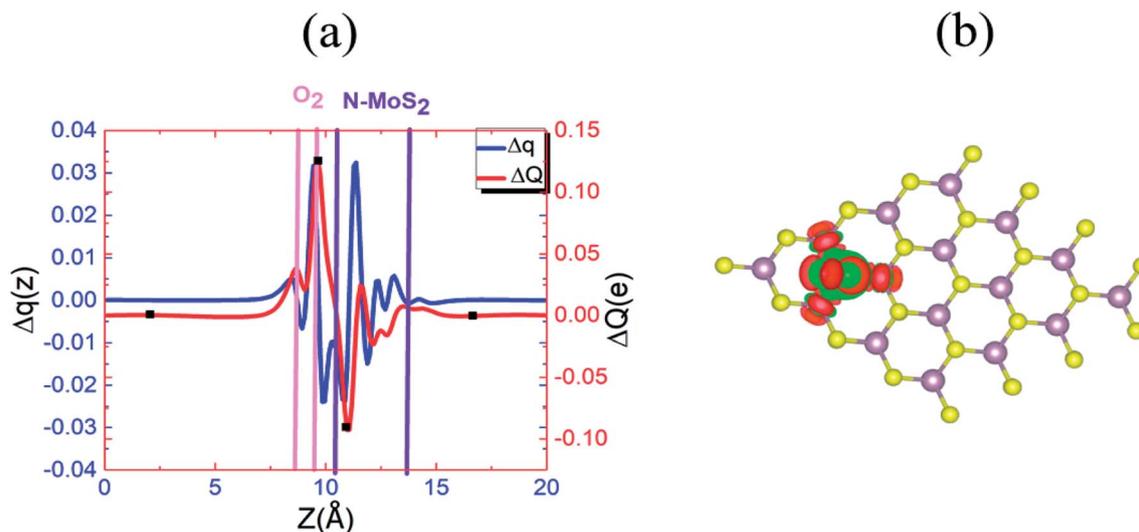
Fig. 4 (a) $\Delta q(z)$ and $\Delta Q(z)$ versus z for N–MoS$_2$–O$_2$, where the z values corresponding to $Q_{min}(z)$ and $Q_{max}(z)$ are shown by filled squares (■). (b) Differential charge density $\Delta \rho(x, y, z)$ contour plot for N–MoS$_2$–O$_2$, where the charge accumulation and depletion regions are represented by red and green colors, respectively.
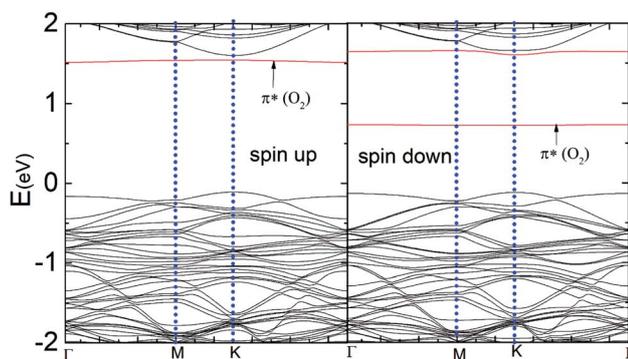

Fig. 5 Band structure of the N–MoS$_2$–O$_2$ complex system for the spin-up and spin-down states.

energy of the O$_2$ molecule on a pristine graphene sheet because it has been demonstrated to have a significant effect on the gas sensor properties. The E_{ad} values are −0.04 and −0.11 eV, respectively,[41] which are larger than that on the pristine MoS$_2$ monolayer using the PBE and PBE-D2 functionals. Meanwhile, the calculated sulfur and oxygen atom distance of 3.38 Å does not indicate the formation of a chemical bond between the sulfur and oxygen atom, which is slightly shorter in the report by Ma et al.[11] The spin-polarized calculation showed that the MoS$_2$–O$_2$ complex system shows a magnetic moment (1.62μ_B), where the spin density transfers to the Mo atom of the MoS$_2$ monolayer. Fig. S4† shows the band structure of the MoS$_2$–O$_2$ system for the spin-up and spin-down states, where the O$_2$ states are introduced above the Fermi level in the spin-down channel absorption of the O$_2$ molecule; thus, the band gap in the spin-down channel absorption is reduced to 1.10 eV. While, the band gap in the spin-up channel absorption is 1.74 eV, which is equal to the value of the pristine single-layer MoS$_2$. Specifically, the binding of an oxygen atom results in a weak p-type effect in the pristine MoS$_2$ monolayer.

The condition was quite distinct and interesting when we adsorbed a gas molecule on the substituted N and P atom (4 × 4) MoS$_2$ monolayer. Table S1† contains the adsorption and relative energy of the O$_2$ molecule on N–MoS$_2$ for distinct configurations. Fig. 3(a) and (b) exhibit the chemical structure of the N–MoS$_2$–O$_2$ complex system. According to the results, the adsorption of an O$_2$ molecule on the MoS$_2$ monolayer in the parallel attachment is more favorable than the vertical attachment. Considering the two different parallel configurations, in configuration P$_1$, two oxygen atoms on the top of the N atom is significantly (1.99 eV) more stable than configuration P$_2$, in which the O$_2$ is molecule located far away from the N atom. Thus, O$_2$ molecule adsorption on N–MoS$_2$ is stronger than that in the pristine MoS$_2$ monolayer. Indeed, the O–O atom distance is 1.27 Å, which indicates the charge distribution from the N-rich MoS$_2$ to the oxygen atom of the O$_2$ molecule is remarkable and the bonds become weaker. In addition, the O$_2$ molecule resides closer to the N–MoS$_2$ plane than that in the pristine MoS$_2$, where the calculated N and oxygen atom distance is 1.68 Å (1.66 Å),[42] which is shorter compared to that in the case of the MoS$_2$–O$_2$ complex. The spin polarization is also intensified on the O$_2$ molecule and the magnetic moment (0.83μ_B) of the system is also reduced. The adsorption energy of the N–MoS$_2$–O$_2$ complex of −0.32 eV (−0.37)[42] is slightly shorter in our calculations. On the other hand, the adsorption energy is appreciably large compared to that in the case of O$_2$ molecule adsorption on N-doped graphene and BC3 graphene-like sheet doped with metal atoms.[41–48] Next, we observed the adsorption of two oxygen molecules on the 2N–MoS$_2$ monolayer, where two N atoms were doped afar to avoid interaction with the O$_2$ gas molecules. Fig. S5(a) and (b)† shows the chemical structure of the 2N–MoS$_2$–2O$_2$ complex. Briefly, the adsorption energy (E_{ad}) on the 2N–MoS$_2$–2O$_2$ complex system is −0.22 eV per oxygen molecule, which is smaller than that of the N–MoS$_2$–O$_2$ complex.
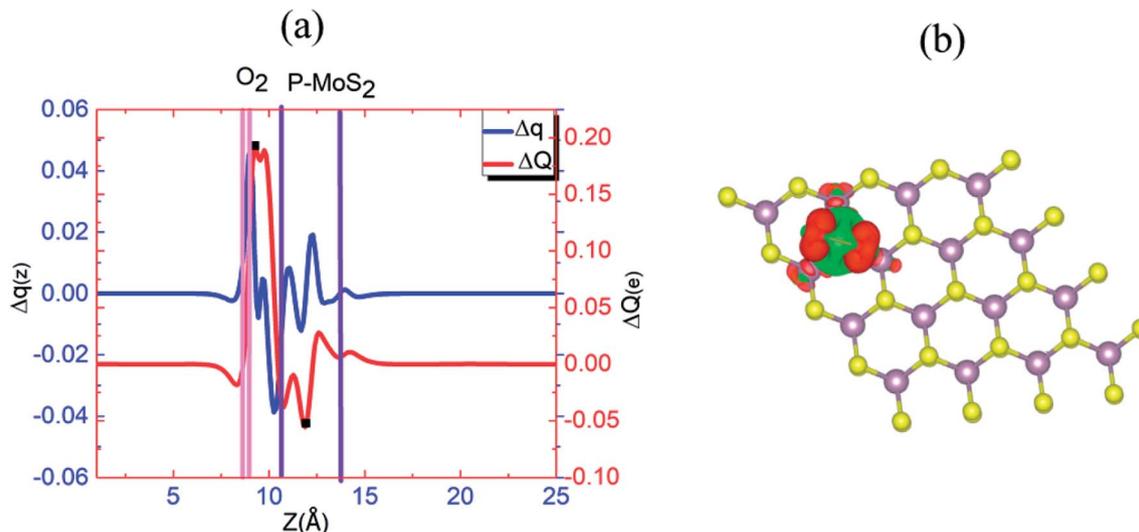
Fig. 6 (a) $\Delta q(z)$ and $\Delta Q(z)$ versus z for P−MoS$_2$−O$_2$, where the z values corresponding to $Q_{min}(z)$ and $Q_{max}(z)$ are shown by filled squares (■). (b) Differential charge density $\Delta\rho(x, y, z)$ contour plot for P−MoS$_2$−O$_2$, where the charge accumulation and depletion regions are represented by red and green colors, respectively.
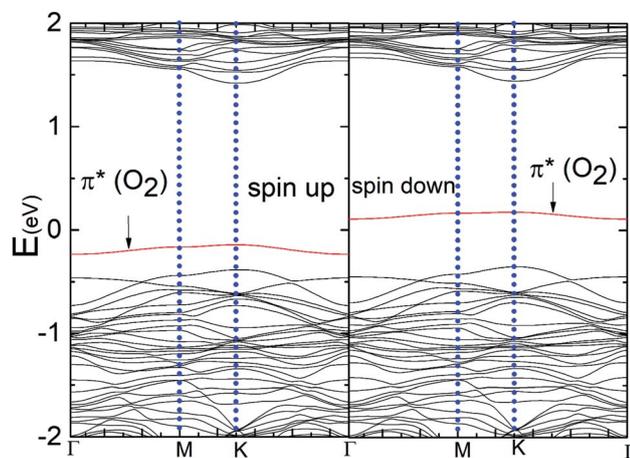

Fig. 7 Band structures of the P−MoS$_2$−O$_2$ complex system for the spin-up and spin-down states.

To understand this observation, we defined the change of the electron density (e Å^{-3}) along the c-axis as $\Delta\rho(z) = \{\rho(z)[N–MoS_2–mO_2] − \rho(z)[N–MoS_2] − \rho(z)[mO_2]\}$. Here, $\rho(z)$ represents the electron density of an appropriate system described in the parentheses, which is averaged over the XY plane in a supercell. This calculation is based on the electron density of the N–MoS$_2$–O$_2$ complex subtracted from that of an isolated N–MoS$_2$ single layer and O$_2$ molecule in the same configurations of the same supercell. We note that the total charge of the complex is zero, although O$_2$ will exist in the form of O$_2^-$ ions after complex formation. Fig. 4(a) shows the $\Delta q(z)$ of the O$_2$ complex in the case of the N–MoS$_2$ system. Here, $\Delta q(z) = \Delta\rho(z)\Delta V$, $\Delta V = V_{cell}/N_c$, and V_{cell} and N_c (=216) are the volumes of the supercell and the number of fine grids along the c-axis, respectively. The thickness of each N–MoS$_2$ layer is defined by the z coordinates of the sulfur atoms in the upper and lower sublayers (S$_L$ and S$_U$,

respectively) with $z(S_L) < z(S_U)$. In each configuration, the thickness of the O$_2^-$ ions is defined by the minimum and maximum of the z coordinates of all the atoms in the ions. The figure shows that there is a significant decrease in the $\Delta q(z)$ in the O$_2$ moiety, signaling the conversion of this moiety to an O$_2^-$ ion. Fig. 4(a) shows that the transferred charge is mainly concentrated on the O$_2$ molecule. For quantitative analysis, we defined the accumulated excess charge as: $Q(z)$: $Q(z) = \sum_{0}^{z' < z} q(z')$. Next, the amount of charge transfer was defined by the relation: $\Delta Q = [Q_{max}(z) − Q_{min}(z)]$. As shown in Fig. 4(a), $Q_{max}(z)$ and $Q_{min}(z)$ correspond to the maxima and minima adjacent to the N–MoS$_2$ layers, respectively. Fig. 4(b) shows contour plots of the differential charge density $\Delta\rho(x, y, z)$, which is not integrated over the XY plane for the N–MoS$_2$–O$_2$ system. The charge accumulation and depletion regions are represented in red and green colors, respectively. The plots reveal a significant electron transfer from the N–MoS$_2$ layer to the O$_2$ molecule. Also, the majority of the transferred electrons are concentrated in the O$_2$ molecule.

Fig. 5 represents the band structure of the N–MoS$_2$–O$_2$ complex system for the spin-up and spin-down states. In this case, the Fermi level shifted 0.23 eV downward, which may appear due to the large charge (0.40e) transfer from the nitrogen-rich MoS$_2$ to the O$_2$ molecule, which is consistent with the larger adsorption energy of O$_2$ on N–MoS$_2$. Due to the intermolecular interaction, the molecular level shifts upward and the spin-polarized π^* state of the O$_2$ molecule is located at 0.72 eV above the VBM, as shown in Fig. 5. The sharp peak of the spin-up at the Fermi level disappears due to large charge transfer or shifted below the Fermi level. Fig. 1(b) indicates the presence of a localized N atom state around the Fermi level in the spin-up and down states, while the absorption of an O$_2$ molecule suppresses these states and it removed the substituted N atom states, as shown in Fig. 5. These findings are
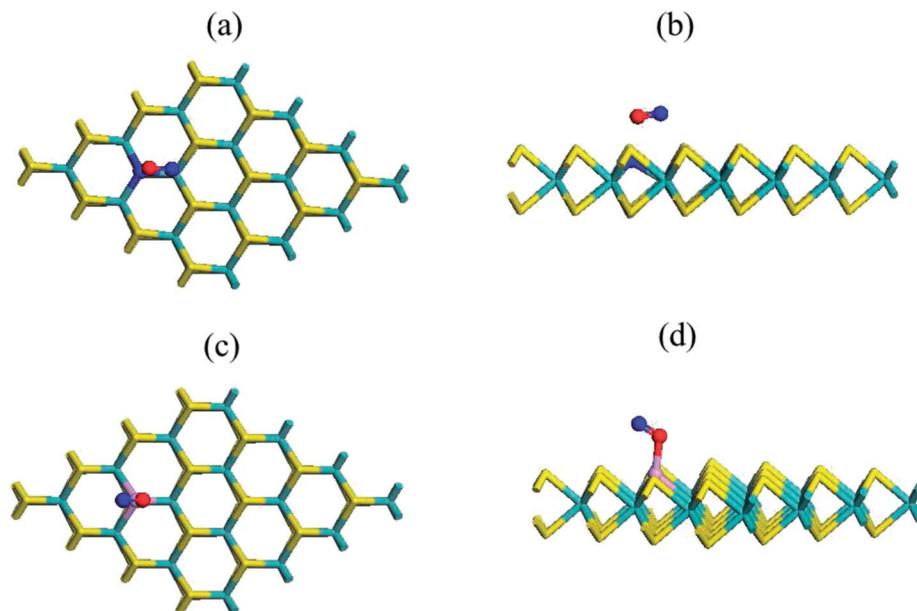
Fig. 8 Top (a and c) and side (b and d) views of the chemical structure of the N- and P-substituted MoS_2−NO complex, where violet, yellow, green, red and purple sticks represent the Mo, S, N, O and P atoms, respectively.

consistent with that observed previously.[39,40] Our PDOS analysis presented in Fig. S6† also confirms that the p-O states are located at 0.05 and 0.07 eV below the CBM in the case of the spin-down and spin-up band structures, respectively. In contrast, the valence band mainly contains a combination of d-Mo and p-S states. Thus the band gaps in the spin-down and spin-up channels are 0.84 eV and 1.66 eV, respectively, which are significantly reduced compared to that in the MoS_2−O_2 system. Therefore, the more negative adsorption energy of the O_2 molecule clearly exhibits oxygen binding introduces a strong p-type effect into the MoS_2 monolayer with N atom substitution.

Considering this, we explored the P−MoS_2 complex, which is distinct from the case of N−MoS_2. Fig. 3(c) and (d) display the

chemical structure of the P−MoS_2−O_2 complex. The P atom forms P−O_1 and P−O_2 bonds with the oxygen atom of the O_2 molecule, which is a partial sp^3 complex. The intended bond lengths are 2.48 Å for Mo−P, 1.66 Å for P−O_1, and 1.64 Å for P−O_2, which agree well with earlier reported values.[42,43] Table 1 exhibits that the adsorption energy per O_2 gas molecule is −1.27 eV, which is significantly larger compared to that of the N−MoS_2−O_2 and MoS_2−O_2 complex systems. Our adsorption energy value is significantly more negative than the earlier reported values (−0.87, −0.93, and −1.11 eV)[42–45] for O_2 adsorption on a P−MoS_2 monolayer. In contrast, the adsorption energy (−1.26 eV)[41] is comparable in the case of O_2 adsorption on a P-doped graphene sheet. The distance between the substituted P

Fig. 9 (a) $\Delta q(z)$ and $\Delta Q(z)$ versus z for N−MoS_2−NO, where the z values corresponding to $Q_{min}(z)$ and $Q_{max}(z)$ are shown by filled squares (■). (b) Differential charge density $\Delta\rho(x, y, z)$ contour plot for N−MoS_2−NO, where the charge accumulation and depletion regions are represented by red and green colors, respectively.
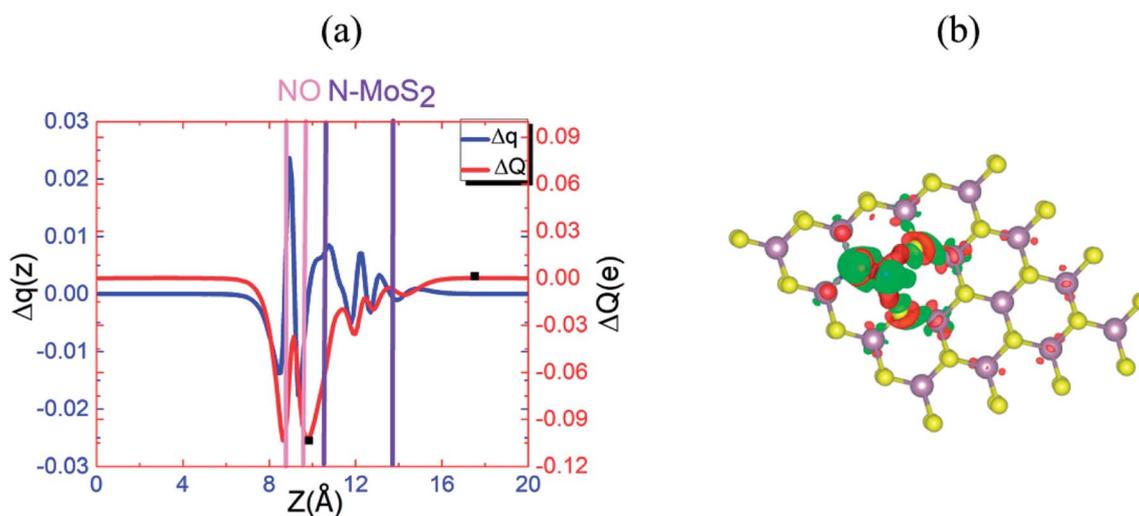
Fig. 10 (a) $\Delta q(z)$ and $\Delta Q(z)$ *versus* z for P–MoS$_2$–NO, where the z values corresponding to $Q_{min}(z)$ and $Q_{max}(z)$ are shown by filled squares (■). (b) Differential charge density $\Delta \rho(x, y, z)$ contour plot for P–MoS$_2$–NO, where the charge accumulation and depletion regions are represented by red and green colors, respectively.
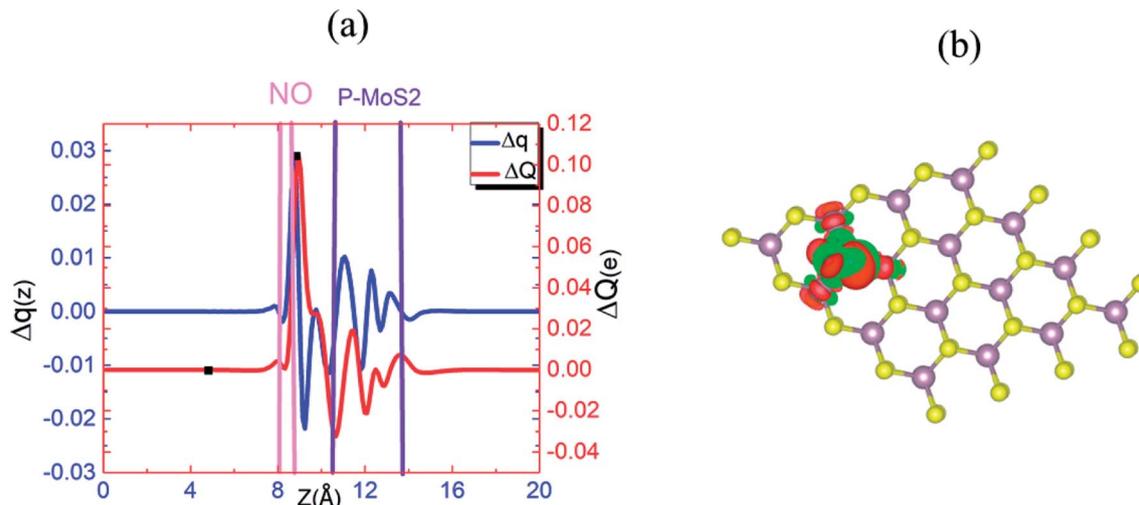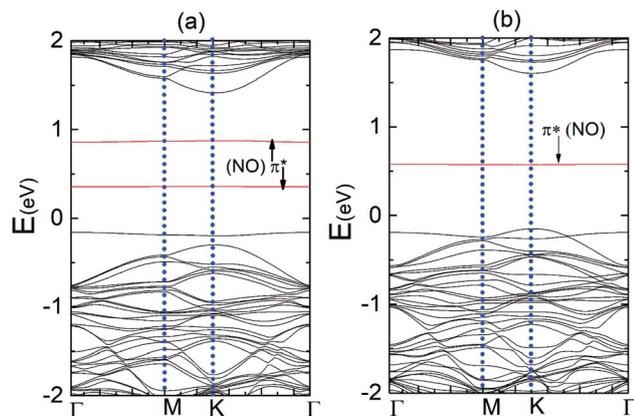

Fig. 11 (a) Band structures of the N–MoS$_2$–NO and (b) P–MoS$_2$–NO complex system, respectively.

atom of MoS$_2$ and oxygen atom of the O$_2$ gas molecule is 1.65 Å, which is slightly shorter compared to the N–O atom distance. In this case, we also examined two different configurations in the parallel (P) attachment, where configuration P$_1$ is significantly (2.07 eV) more stable than configuration P$_2$, in which the two oxygen atoms are far from the dopant atom. Subsequently, we determined the adsorption of two O$_2$ gas molecules on the 2P–MoS$_2$ monolayer and Fig. S5(c) and (d)† show the chemical structure of the 2P–MoS$_2$–2O$_2$ complex. In this case, the calculated adsorption energy is −1.22 eV per O$_2$ molecule, which is comparable with that of the above-described P–MoS$_2$–O$_2$ complex system. The spin-polarized calculation shows that the systems become magnetic with 0.80 and 1.62μ_B, respectively, which confirms the spin density transferred to the Mo atom of the P–MoS$_2$ monolayer.

Fig. 6(a) and (b) show the $\Delta q(z)$ and contour plots $\Delta \rho(x, y, z)$ for the O$_2$ complex in case of the P–MoS$_2$ system. This figure shows that there is a significant decrease in $\Delta q(z)$ in the O$_2$

moiety and 0.25e charge transfer from the P–MoS$_2$ monolayer to the gas molecule. It also displays that the transferred charge is mainly concentrated in the interlayer region adjacent to the O$_2$ molecule, where the charge accumulation and depletion regions are represented in red and green, respectively. Subsequently, we explored the electronic properties of an O$_2$ molecule adsorbed on P–MoS$_2$ and calculated the band structure for the spin-up and spin-down states, as shown in Fig. 7. The presence of the localized state of P atom around the Fermi level in the spin-up and down states in the band structure of P–MoS$_2$ was observed, while the absorption of an O$_2$ molecule suppressed these stated and removed the P atom states, as shown in Fig. 7. On the other hand, the two spin-polarized π^* states of the O$_2$ molecule were introduced above and below the Fermi level in the spin-down and spin-up bands, which may be appear due to charge transfer from the substrate to the absorbed O$_2$ molecule, as presented in Fig. S6.† The charge transfer to the spin-up and spin-down bonding and anti-bonding π^* states is the origin of the significant elongation of the O–O (1.57 Å) bond. The enlargement of the O–O bond due to charge transfer indicates the significant weakening of the O–O bond and signals the conversion of this moiety to the O$_2^-$ ion on the surface of the P–MoS$_2$ monolayer. These findings are highly desirable for chemical reactions, such as the oxidation of CO, since breaking of O$_2$ bonds is consider the key rate-limiting step.[13]

Here, our aim was to investigate the adsorption of NO gas on the pristine and N–MoS$_2$ monolayer. The calculated adsorption energy is −0.26 eV per NO molecule, and the sulfur and N atom distance of 3.03 Å indicates that it can be physisorbed on the pristine MoS$_2$ monolayer. The tabulated adsorption energy agrees well with the reported theoretical calculations.[13–30] The length of the N–O bond of 1.17 Å remains the same as that in the isolated NO molecule in the gas phase, which shows good agreement with the reported values.[11–28] Here, it is also important to compare the adsorption energy of an NO molecule on a pristine monolayer graphene. The adsorption energies are

(−0.03 and −0.12 eV),[41] which is significantly smaller than that on the pristine MoS_2 monolayer. Fig. 8(a) and (b) display the chemical structure of the $N-MoS_2-NO$ complex and Table S2† compares the adsorption energies for different configurations of the NO molecule, which shows that configuration P_1 is more stable. Table 1 compares the adsorption energy of the N-doped and pristine MoS_2 monolayer, which distinctly indicates that NO adsorption is stronger on the $N-MoS_2-NO$ complex system. Also, the adsorption energy of the $N-MoS_2-NO$ complex is more negative than the reported values for N and metal atom-doped graphene.[41,49] Therefore, the length of the N–O bond decreases to 1.15 Å and the distance between $N-MoS_2$ and the NO molecule of 2.18 Å shows strong binding between the adsorbate and absorbent. Next, we investigated the adsorption of two NO gas molecules on the $2N-MoS_2$ monolayer and the determined adsorption energy was −0.37 eV per NO molecule. Fig. S8(a) and (b)† represent the chemical structure of the $2N-MoS_2-2NO$ complex. Therefore, the adsorption energy result indicates that $2N-MoS_2$ monolayer systems are not appropriate for gas sensing and are weakly bonded compared to the $N-MoS_2-O_2$ complex.

Fig. 9(a) and (b) display the $\Delta q(z)$ and contour plots $\Delta \rho(x, y, z)$ for the NO complex in the case of the $N-MoS_2$ monolayer. This figure displays that $0.11e$ charge transfers from $N-MoS_2$ to the NO molecule, so there is a significant decrease in $\Delta q(z)$ in the NO moiety, indicating the conversion of this moiety to an NO^- ion. It shows that the transferred charge is mainly concentrated in the region adjacent to the NO molecule, where the charge accumulation and depletion regions are represented in red and green, respectively. Fig. 11(a) shows the band structure of the $N-MoS_2-NO$ complex system, which indicates that NO adsorption causes the system to become nonmagnetic semiconductor and this is clearly different from the case of O_2 molecule adsorption. Our density of states (DOS) analysis presented in Fig. S9† shows that a localized state below the Fermi level appears due to the strong Mo–N bonding and transfer of charge from Mo to the N atom. The two localized π^* states of the NO molecule are introduced at 0.35 and 0.87 eV below the conduction band minimum. These two localized π^* states are split due to the charge transfer from $N-MoS_2$ monolayer to NO gas molecule.

Here, we explored the adsorption of an NO molecule on the $P-MoS_2$ monolayer. Table S2† compares the adsorption energies for the different possible configurations of NO molecule, which indicates P_1 is the most stable configuration. The configuration in which the P–N bond formed is more stable (0.79 eV) compared to the case of the P–O bond configuration. In this case, the calculated adsorption energy of −1.44 eV per molecule is larger than that of the $N-MoS_2-NO$, $N-MoS_2-O_2$, and $P-MoS_2-O_2$ complex systems. Furthermore, the binding is also stronger than that of the MoS_2-O_2 and MoS_2-NO complex systems. Moreover, our result of adsorption energy for the NO molecule is significantly larger than the reported value (−0.61 eV)[41] for P-doped graphene obtained using PBE-D2 calculations and the adsorption energy (0.91, 0.96 and 1.38 eV)[17] of the metal-atom doped MoS_2 monolayer. In contrast, the adsorption energy of an NO gas molecule on a metal atom-modified BC3 sheet is also smaller compared to that of the $P-MoS_2-NO$ and

$N-MoS_2-NO$ complex systems.[50,51] Fig. 8(c) and (d) present the geometry of the $P-MoS_2-NO$ complex, which is in accordance with this result and shows that it can be thought of as a weak P–N bond with a length of 1.93 Å. This bond is formed due to the secondary interaction of the π^* states of the NO molecule with the P atom atomic orbital. The N–O bond length of 1.20 Å is not significantly elongated upon adsorption as in case the of the O_2 molecule. Fig. S8 (c) and (d)† represent the chemical structure of the $2P-MoS_2-2NO$ complex, where the adsorption energy is −1.38 eV, which is comparable with the previously described complex system.

Fig. 10(a) and (b) present the $\Delta q(z)$ and contour plots $\Delta \rho(x, y, z)$ for the NO complex in the case of the $P-MoS_2-NO$ system. It indicates that slightly more charge is transferred from the $P-MoS_2$ monolayer to NO molecule than the $N-MoS_2-NO$ and MoS_2-NO complex systems. It also describes a more negative adsorption energy due to the large charge transfer from the adsorbate to the absorbent. This observation clearly indicates a strong p-type effect appears due to the large transfer of an electron and confirms the chemisorption of the NO molecule on the $P-MoS_2$ monolayer. Fig. 11(b) presents the band structure of the $P-MoS_2-NO$ complex system. The (PDOS) analysis shown in Fig. S10† indicates that the NO adsorption leaves nonmagnetic semiconductor character in the P- and N-substituted MoS_2 monolayer. The localized state below the Fermi level appears due to strong Mo–P bonding and π^* states of the NO molecule located at 0.56 eV above the valence band maximum. The Fermi level shifted upward by 0.29 eV in the case of the $P-MoS_2-NO$ complex system as a result of $0.14e$ charge transfer from the $P-MoS_2$ monolayer to an NO gas molecule.

4. Conclusion

We performed first principle calculation inspection of O_2 and NO gas molecules adsorbed on pristine MoS_2, N-doped, and P-doped MoS_2. The excellent agreement of the adsorption energy with earlier reported data distinctly shows the validity of our PBE-D3 calculation in describing the van der Waals interaction. We found that the adsorption is stronger on N-doped and P-doped MoS_2 compared to the case of the pristine MoS_2 monolayer. In the case of N-doped MoS_2 with O_2 or NO molecules, the spins of the two adsorbed molecules couple differently depending upon the type of adsorbed gas molecule. When the former molecule was adsorbed, ferromagnetic coupling was observed, while the spins coupled antiferromagnetically when the latter molecule was absorbed. These findings suggest that the magnetic properties of $N-MoS_2$ may be used for the quantitative sensing of O_2 gas. The adsorption of these gases on $P-MoS_2$ is stronger than that on the $N-MoS_2$ monolayer. The adsorption of O_2 molecules leaves $P-MoS_2$ a magnetic semiconductor, while the adsorption of NO molecules turns this system into a nonmagnetic semiconductor. Therefore, P-doped and N-doped MoS_2 can be used to distinguish between O_2 and NO gases using magnetic properties. Therefore, $P-MoS_2$ based gas sensors are predicted to be more sensitive to detect NO and O_2 molecules than pristine or N-doped MoS_2. Hence, $P-MoS_2$ gas sensors are more suitable for detecting NO molecules due to

their stronger adsorption energy and are less suitable for detecting O_2 molecules due to their smaller adsorption energy.

Conflicts of interest

There are no conflicts of interest.

Acknowledgements

References

1 A. H. Castro Neto, F. Guinea, N. M. R. Peres, K. S. Novoselov and A. K. Geim, *Rev. Mod. Phys.*, 2009, **81**, 109–162.

2 G. Eda and M. Chhowalla, *Adv. Mater.*, 2010, **22**, 2392–2415.

3 B. Robert, *Sens. Rev.*, 2015, **35**, 1–5.

4 Y. Liu, X. Dong and P. Chen, *Chem. Soc. Rev.*, 2012, **41**, 2283–2307.

5 A. Kuc, N. Zibouche and T. Heine, *Phys. Rev. B: Condens. Matter Mater. Phys.*, 2011, **83**, 245213.

6 Y. Huang, J. Guo, Y. Kang, Y. Ai and C. M. Li, *Nanoscale*, 2015, **7**, 19358–19376.

7 Q. He, Z. Zeng, Z. Yin, H. Li, S. Wu, X. Huang and H. Zhang, *Small*, 2012, **8**, 2994–2999.

8 H. Li, Z. Yin, Q. He, H. Li, X. Huang, G. Lu, H. Fam Derrick Wen, Y. Tok Alfred Iing, Q. Zhang and H. Zhang, *Small*, 2011, **8**, 63–67.

9 O. Leenaerts, B. Partoens and F. M. Peeters, *Phys. Rev. B: Condens. Matter Mater. Phys.*, 2009, **79**, 235440.

10 W. T. Cong, Z. Tang, X. G. Zhao and J. H. Chu, *Sci. Rep.*, 2015, **5**, 9361.

11 D. Ma, Q. Wang, T. Li, C. He, B. Ma, Y. Tang, Z. Lu and Z. Yang, *J. Mater. Chem. C*, 2016, **4**, 7093–7101.

12 D. Ma, W. Ju, T. Li, G. Yang, C. He, B. Ma, Y. Tang, Z. Lu and Z. Yang, *Appl. Surf. Sci.*, 2016, **371**, 180–188.

13 Q. Yue, Z. Shao, S. Chang and J. Li, *Nanoscale Res. Lett.*, 2013, **8**, 425.

14 J. Dai and J. Yuan, *Phys. Rev. B: Condens. Matter Mater. Phys.*, 2010, **81**, 165414.

15 Z. Miao, L. Yun-Hao, C. Yong-Qing, Z. Chun and F. Yuan-Ping, *Nanotechnology*, 2011, **22**, 385502.

16 D. Ma, Y. Tang, G. Yang, J. Zeng, C. He and Z. Lu, *Appl. Surf. Sci.*, 2015, **328**, 71–77.

17 D. Ma, W. Ju, T. Li, X. Zhang, C. He, B. Ma, Z. Lu and Z. Yang, *Appl. Surf. Sci.*, 2016, **383**, 98–105.

18 B. B. Xiao, P. Zhang, L. P. Han and Z. Wen, *Appl. Surf. Sci.*, 2015, **354**, 221–228.

19 J. He, K. Wu, R. Sa, Q. Li and Y. Wei, *Appl. Phys. Lett.*, 2010, **96**, 082504.

20 H. Zheng, B. Yang, D. Wang, R. Han, X. Du and Y. Yan, *Appl. Phys. Lett.*, 2014, **104**, 132403.

21 W. Ju, T. Li, X. Su, H. Li, X. Li and D. Ma, *Phys. Chem. Chem. Phys.*, 2017, **19**, 20735–20748.

22 L.-p. Feng, J. Su and Z.-t. Liu, *J. Alloys Compd.*, 2014, **613**, 122–127.

23 I. S. Kwon, I. H. Kwak, H. G. Abbas, Y. Lee, G. Jung, S. J. Yoo, J.-G. Kim, J. Park and H. S. Kang, *Nanoscale*, 2018, **10**, 11349–11356.

24 I. H. Kwak, I. S. Kwon, H. G. Abbas, G. Jung, Y. Lee, J. Park and H. S. Kang, *J. Mater. Chem. A*, 2018, **6**, 5613–5617.

25 H.-P. Komsa, J. Kotakoski, S. Kurasch, O. Lehtinen, U. Kaiser and A. V. Krasheninnikov, *Phys. Rev. Lett.*, 2012, **109**, 035503.

26 W. Zhou, X. Zou, S. Najmaei, Z. Liu, Y. Shi, J. Kong, J. Lou, P. M. Ajayan, B. I. Yakobson and J.-C. Idrobo, *Nano Lett.*, 2013, **13**, 2615–2622.

27 H. Li, M. Huang and G. Cao, *Phys. Chem. Chem. Phys.*, 2016, **18**, 15110–15117.

28 C. González, B. Biel and Y. J. Dappe, *Phys. Chem. Chem. Phys.*, 2017, **19**, 9485–9499.

29 S.-Y. Cho, S. J. Kim, Y. Lee, J.-S. Kim, W.-B. Jung, H.-W. Yoo, J. Kim and H.-T. Jung, *ACS Nano*, 2015, **9**, 9314–9321.

30 S. Zhao, J. Xue and W. Kang, *Chem. Phys. Lett.*, 2014, **595–596**, 35–42.

31 H. Qiu, L. Pan, Z. Yao, J. Li, Y. Shi and X. Wang, *Appl. Phys. Lett.*, 2012, **100**, 123104.

32 L. Qiuhong, W. Xia, W. Zhenjun, H. Jia, L. Dongdong, W. Qiang and W. Shuangyin, *Nanotechnology*, 2016, **27**, 175402.

33 H. Huang, X. Feng, C. Du and W. Song, High-quality phosphorus-doped MoS2 ultrathin nanosheets with amenable ORR catalytic activity, *Chem. Commun.*, 2015, **51**(37), 7903–7906.

34 G. Kresse and J. Hafner, *Phys. Rev. B: Condens. Matter Mater. Phys.*, 1993, **47**, 558–561.

35 G. Kresse and J. Furthmüller, *Phys. Rev. B: Condens. Matter Mater. Phys.*, 1996, **54**, 11169–11186.

36 G. Kresse and D. Joubert, *Phys. Rev. B: Condens. Matter Mater. Phys.*, 1999, **59**, 1758–1775.

37 S. Grimme, *J. Comput. Chem.*, 2006, **27**, 1787–1799.

38 J. N. Dimple and S. Abir De, *J. Phys.: Condens. Matter*, 2017, **29**, 225501.

39 A. Brahim, P. Ruth and M. Shin, *Nanotechnology*, 2016, **27**, 185701.

40 H. Okamoto, R. Schilling, H. Schütz, V. Sudhir, D. J. Wilson, H. Yamaguchi and T. J. Kippenberg, *Appl. Phys. Lett.*, 2016, **108**, 153105.

41 A. Pramanik and H. S. Kang, *J. Phys. Chem. C*, 2011, **115**, 10971–10978.

42 H. Zhang, Y. Tian, J. Zhao, Q. Cai and Z. Chen, *Electrochim. Acta*, 2017, **225**, 543–550.

43 S. Zhao, J. Xue and W. Kang, *Chem. Phys. Lett.*, 2014, **595–596**, 35–42.

44 C. Liu, H. Dong, Y. Ji, T. Hou and Y. Li, *Sci. Rep.*, 2018, **8**, 13292.

45 X. Zhang, S. Shi, T. Gu, L. Li and S. Yu, *Phys. Chem. Chem. Phys.*, 2018, **20**, 18184–18191.

46 Y. Tang, H. Chai, H. Zhang, W. Chen, W. Zhang and X. Dai, *Phys. Chem. Chem. Phys.*, 2018, **20**, 14040–14052.

47 H. Zhang, Y. Tang, Y. Ma, D. Ma, M. Zhao and X. Dai, *Appl. Surf. Sci.*, 2018, **427**, 376–386.

48 Y. Tang, W. Chen, Z. Shen, S. Chang, M. Zhao and X. Dai, *Carbon*, 2017, **111**, 448–458.

49 Y. Tang, Z. Liu, Z. Shen, W. Chen, D. Ma and X. Dai, *Sens. Actuators, B*, 2017, **238**, 182–195.

50 Y. Tang, X. Cui, W. Chen, D. Zhu, H. Chai and X.-Q. Dai, A theoretical study on metal atom-modified BC3 sheets for effects of gas molecule adsorptions, *Appl. Phys. A*, 2018, **6**, 124–434.

51 Y. Tang, M. Zhang, W. Chen, X. Cui, Y. Li and X. Dai, *J. Phys. Chem. Solids*, 2018, **121**, 247–255.